Journal of
Ship&Ocean Technology
© MARCH 2000

SOTECH Vol. 4, No. 1, pp. 11~20, 2000

A Computational Study on Turbulent Flows around Single and Tandem Two-Dimensional Hydrofoils with Shallow Submergence

H.-T. Kim[1], J.-B. Park[1] and W.-J. Kim[2]

[1] Chungnam National University, Taejon, Korea; E-mail: h-tkim@cnu.ac.kr
[2] Korea Research Institute of Ships and Ocean Engineering, Taejon, Korea

Abstract

Reynolds-averaged Navier-Stokes equations are numerically solved using a second-order finite difference method for the analysis of turbulent flows around single and tandem hydrofoils advancing under the free surface. The location of the free surface, not known *a priori*, is computed from the kinematic free surface condition and the computational grid is conformed at each iteration to the free surface deformation. The eddy viscosity model of Baldwin-Lomax is employed for the turbulence closure. The method is validated through the comparison of the numerical results with the experimental data for a single hydrofoil of a Joukowski foil section. A computational study is also carried out to investigate the effect of the submergence depth and the Froude number on the lift and the drag of the hydrofoil. For tandem hydrofoils, computations are performed for several separation distances between the forward and aft foils to see the interference effect. The result shows clearly how the lift and drag change with the separation distance.
Keywords: tandem hydrofoils, free surface, drag and lift, interference effects

1 Introduction

Flow fields around a shallowly submerged hydrofoil advancing at a constant speed are strongly influenced by the waves generated on the free surface. A number of experimental, theoretical and computational studies have been done to analyze and predict the lift and the surface pressure of, as well as the waves generated by, a single hydrofoil. Kochin(1951) obtained some analytic results for the lift and the wave drag of a hydrofoil using the theory of analytic functions under the assumption of large submergence. Parkin, Perry and Wu(1955), hereafter denoted as PPW, made an extensive and important experimental work, in which the surface pressure distributions of a hydrofoil of a Joukowski foil section were measured for various cases of the Froude number(F_n) and the submergence depth. Duncan(1983) carried out an experimental study through which he measured the free surface elevations generated by a hydrofoil of NACA 0012 section and reported the steady breaker following the hydrofoil was produced when the slope of the wave was 17^o or higher. Bai(1978) obtained potential flow solutions for the cases of the experimental setup of

PPW by using a localized finite-element method and later Bai and Han(1994) improved their previous results by implementing the nonlinear free surface condition. Hino(1989) solved the Euler and Navier-Stokes equations using a finite difference method for the solutions of the NACA 0012 foil section corresponding to the experiments of Duncan(1983). Shin and Mori(1989) calculated the same flows including the effect of viscosity. Kim and Van(1995) carried out an experimental and computational study on the flow around a hydrofoil of NACA 0012 section. In the experiment, the free surface elevation and the surface pressure were measured at the same time. Lee and Kim(1996) made a theoretical and computational work on the lift of and wave breaking behind a shallowly submerged body and proposed the two-parameter plane which could be used for predicting the possibility of wave breaking behind the submerged body. Recently, Van, Kim and Kim(Van et al 1996) investigated the lift characteristics for submerged hydrofoils moving under the free surface by both the potential flow analyses and the turbulent flow calculations. Although there have been a lot of studies on a single hydrofoil as mentioned above, the study on tandem hydrofoils is very rare at least to the authors' knowledge. In the present study, the finite difference method of Kim and Van (1995) has been extended for the analysis of turbulent flows around tandem hydrofoils advancing at a constant speed under the free surface with a shallow submergence. For the validation of the present method, the comparison of the numerical results for a single hydrofoil with the experimental data of PPW(Parkin et al 1955) is first given. For tandem hydrofoils, computations are carried out for several separation distances between the forward and aft foils to investigate their interference effect.

2 Numerical Methods

As abovementioned, the finite difference method of Kim and Van(1995) has been extended for the case of two hydrofoils in a tandem arrangement. Since the computational method was described in details in Kim(1994), only a brief outline of the method is given herein.

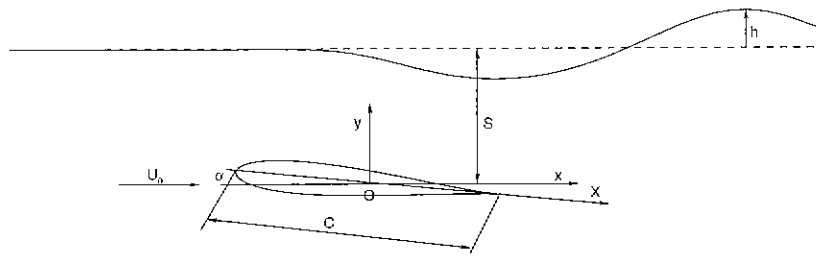

Figure 1: Coordinate system

2.1 Governing equations

In the Cartesian coordinates, whose origin is at the midchord of the hydrofoil, x-axis parallel to the uniform inflow and y-axis directed opposite to the gravitation, as shown in Figure 1, the Reynolds-

averaged Navier-Stokes equations for the two-dimensional turbulent flow of an incompressible fluid with an isotropic eddy viscosity model can be written in Cartesian tensor notation as follows:

$$\frac{\partial u_k}{\partial x_k} = 0 \tag{1}$$

$$\frac{\partial u_i}{\partial t} + u_j \frac{\partial u_i}{\partial x_j} = -\frac{\partial}{\partial x_i}(\hat{p}) + \frac{1}{R_{eff}} \frac{\partial^2 u_i}{\partial x_k \partial x_k} + \frac{\partial \nu_t}{\partial x_j}(\frac{\partial u_j}{\partial x_i} + \frac{\partial u_i}{\partial x_j}) \tag{2}$$

where the mean velocity components $u_i = (u, v)$, the coordinates $x_i = (x, y)$, the inverse of the effective Reynolds number $\frac{1}{R_{eff}} = \frac{1}{R_e} + \nu_t$, and a modified pressure $\hat{p} = p + \frac{y}{F_r^2} + \frac{2}{3}k$. The equations are nondimensionalized by the chord length of the hydrofoil C, the speed of the inflow U_0, and the fluid density ρ. The Reynolds and Froude numbers are defined as $R_e = U_0 C/\nu$ and $F_r = U_0/\sqrt{gC}$, respectively, where ν is the kinematic viscosity of the fluid and g the gravitational acceleration. In the present study, the eddy viscosity, ν_t, is obtained by the turbulence model of Baldwin-Lomax(1978) and the turbulent kinetic energy k is included in the modified pressure to sustain the constitutive equation in the zero-equation turbulence model.

For the computation of flows in a physical domain of arbitrary geometry, the governing equations in the Cartesian coordinates (x, y) are transformed into general body-fitted coordinates (ξ, η). The transformed governing equations are given as follows:

$$\frac{1}{J}\frac{\partial}{\partial \xi^m}(JU^m) = \frac{1}{J}\frac{\partial}{\partial \xi^m}(b_i^m u_i) = 0 \tag{3}$$

$$\frac{\partial u_i}{\partial t} + U^k \frac{\partial u_i}{\partial \xi^k} = -\frac{1}{J} b_i^k \frac{\partial \hat{p}}{\partial \xi^k} + \frac{1}{R_{eff}} \nabla^2 u_i + (\frac{1}{J} b_j^k \frac{\partial \nu_t}{\partial \xi^k})[(\frac{1}{J} b_i^m \frac{\partial u_j}{\partial \xi^m}) + (\frac{1}{J} b_j^m \frac{\partial u_i}{\partial \xi^m})] \tag{4}$$

where the contravariant velocity components are defined by $U^k = b_j^k u_j / J$ and the definition of geometric coefficients are given in the reference(Kim 1994).

2.2 Discretization and pressure-velocity coupling

To solve momentum equations numerically, convection terms are discretized by the third order upwind-biased differencing, diffusion terms by second order central differencing and the Euler-implicit method is applied for the temporal integration of the equations. The discretized momentum equations are solved by using ADI method. The implicit method in each direction results in a set of simultaneous algebraic equations with the penta-diagonal coefficient matrices, for which a highly vectorized solver is available if the pressure field is known. However, as the pressure field is not known *a priori*, it must be determined so that the continuity equation is also satisfied. The pressure-Poisson equation, derived from the continuity equation, is solved to obtain the pressure ensuring the divergence-free velocity field. In the present study, the non-staggered grid system is used and a discrete pressure-Poisson equations, designed to eliminate the checkerboard instability, is solved to satisfy the discrete continuity up to an artificial dissipation term, which is sufficient to avoid the even-odd decoupling of the pressure nodes and guarantee smoothness of the computed pressure field. For more details the reader is referred to the reference(Sotiropoulos 1991).

2.3 Boundary conditions

The boundaries of the physical domain consist of the inlet, the bottom surface, the body boundary, the exit and the free surface. In the present study, two-block H-grid topology is employed. The upper block includes the free surface and the upper side of a hydrofoil and the lower block includes the bottom and the lower side of the hydrofoil. Along the block interface four grid points(two from each side of the block) are overlapped to ensure the continuous change of flow variables across the block interface. The boundary conditions on each of the boundaries are as follows. On the inlet, the uniform flow conditions are specified, i.e., $u = U_0, v = \hat{p} = 0$. On the foil surface, the no-slip condition is imposed, i.e., $u = v = \partial\hat{p}/\partial n = 0$ (where n is normal to the surface). For the bottom boundary, the symmetry condition is applied to account the effect of the restricted water channel in the experiment. Velocity components are extrapolated on the exit. On the free surface, whose location is determined as part of the solution, nonlinear inviscid free-surface conditions are imposed, i.e., the dynamic conditions $\partial(u, v)/\partial y = 0, \hat{p} = h/{F_r}^2$ with the free surface elevation h determined from the solution of the kinematic condition discretized in the finite-difference form

$$\frac{(h^{n+1} - h^n)}{\Delta t} + u^{n+1}(\frac{\partial h}{\partial x})^{n+1} - v^{n+1} + \gamma(x) \quad = \quad 0 \quad at \quad y = h^n(x) \tag{5}$$

where the artificial damping function $\gamma(x)$ is introduced to suppress the reflection of generated waves from the downstream. Following Hino(1993), the quadratic form of the damping function is adopted, i.e., $\gamma(x) = A(\frac{x-x_d}{x_e-x_d})^2 h(x)$ for $x_d \leq x \leq x_e$ and $\gamma(x) = 0$, otherwise. Here, A is a constant controling the amount of damping, x_e the x-coordinate of the exit and x_d is defined such as $x_d = x_e - 2\pi {F_r}^2$. It should be noticed that the damping zone is set about one wave length from the exit boundary. In the present study, $(\frac{\partial h}{\partial x})^{n+1}$ is approximated using the quadratic interpolation in the upwind direction and A of 10 is used. The h is set zero at the inlet and extrapolated at the exit. At each time step, the grid of the upper block is reconstructed to conform the newly obtained free surface elevation while the inviscid dynamic conditions are imposed on the updated free surface.

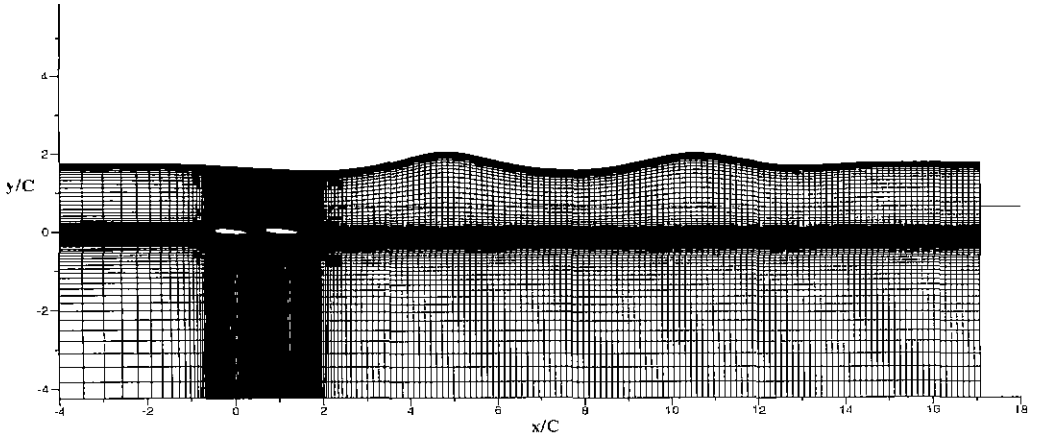

Figure 2: Computational grid system

3 Result and Discussion

The present solution method is applied for the calculation of turbulent flows around a single and tandem hydrofoils of a 12% thick Joukowski section. For all the cases presented here, the angle of attack of the hydrofoil is set 5^o. A body-fitted grid is generated by using the elliptic grid generation method of Visbal and Knight(1982) and the details can be found in Kim(1994). A two-block H-grid topology is employed in which the upper block includes the free surface and the upper side of a hydrofoil and the lower block includes the bottom and the lower side of the hydrofoil. Figure 2 shows a typical computational grid. Grid points are clustered near the hydrofoil surface as well as the free surface. In the following, the results are presented first for the single hydrofoil. Then, the computed results of tandem hydrofoils are described.

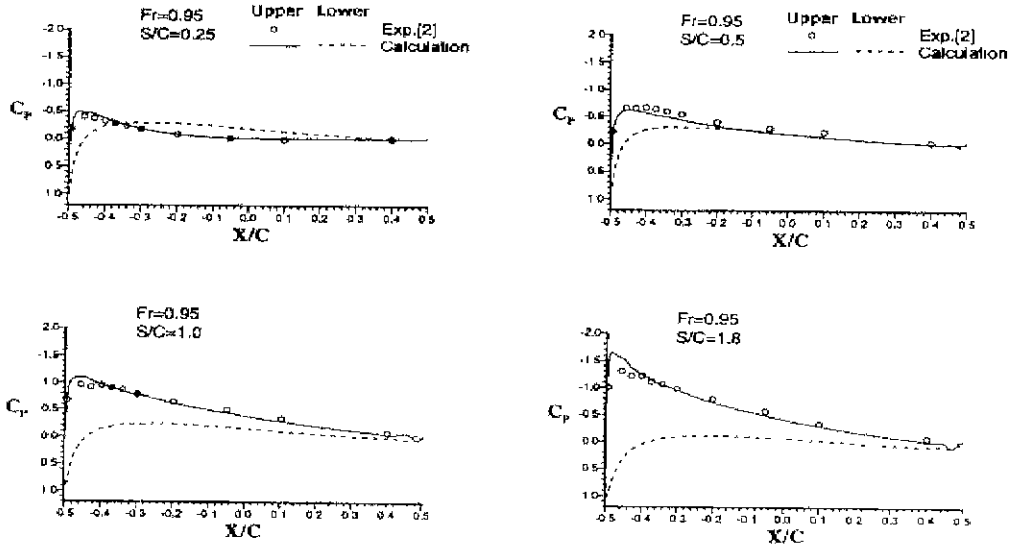

Figure 3: Surface pressure distribution ($F_r = 0.95$)

3.1 Single hydrofoil

In order to show the capability of the present method, some of the results for the surface pressure distributions, which were given in Figure 9 of the reference(Kim and Van 1995), are reproduced in Figure 3. The angle of attack α is 5^o, the Froude number F_r is 0.95 and the Reynolds number is 2.39×10^5. The calculated surface pressures agree well with experiment. It is clearly shown the pressure on the upper(suction) side increases as the depth of submergence decreases and the lift of the hydrofoil decreases consequently. Figure 4 shows the surface pressure distributions for various Froude numbers (F_r= 0.604, 0.632, 0.821, 0.929, 0.984, 1.072) but with the fixed submergence depth($S/C = 0.25$). The calculated results are generally in good agreement with the experiment of PPW(Parkin et al 1955) except for the cases of F_r = 0.604 and 0.632 where the computed pressures on the upper side show large differences from the measurements. These difference may

be due to the wave breaking, which cannot be treated by the present computational method. At this submergence depth, the hydrofoil produces a negative lift for Froude numbers lower than 1 and a very small lift even for Froude numbers much higher than 1.

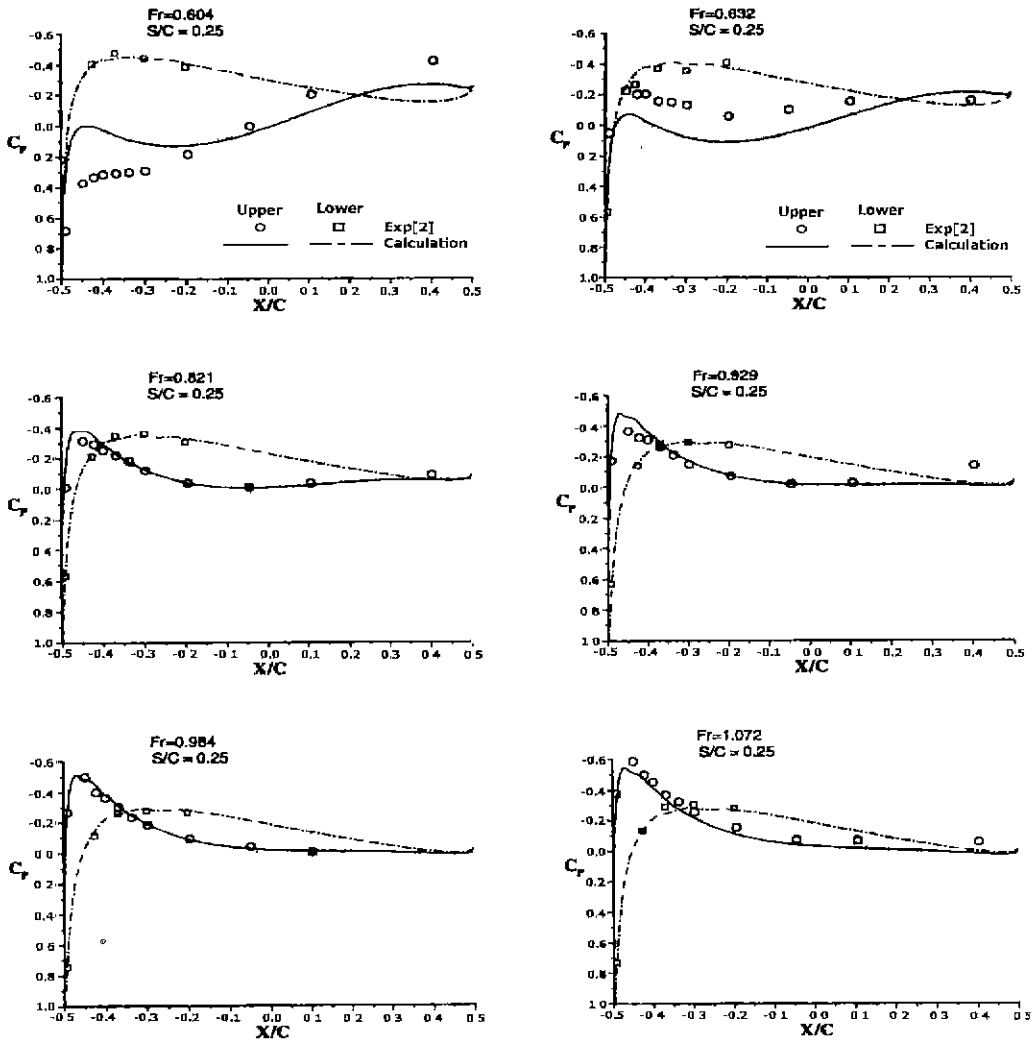

Figure 4: Surface pressure distribution for various Froude number

Figures 5 and 6 present, respectively, the change of the lift and drag coefficients for various submergence depths and Froude numbers. It is shown clearly that the lift of the hydrofoil decreases as the depth of submergence decreases. The lift approaches to its limit of infinite submergence with the smaller submergence depth, the lower the Froude number is. Note the well-known fact that the wave length(λ) is proportional to $2\pi {F_r}^2 C$ and the free surface effect almost vanishes at $S = 0.5\lambda$. For $F_r = 1.414$, the drag decreases as the submergence depth decreases. For $F_r = 0.821$ and 0.95 the drag reaches to its maximum at about $S/C = 0.9$ and it decreases as the depth of submergence either decreases or increases from the maximum point. The trend is similar for $F_r = 0.632$, except the value at $S/C = 0.5$.

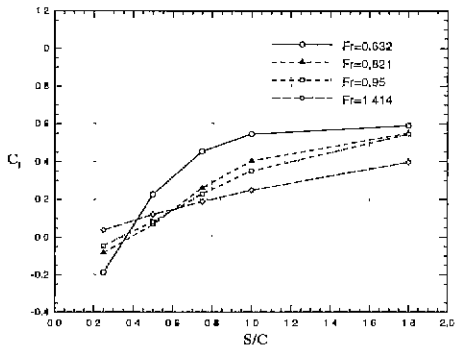

Figure 5: Lift coefficient vs. depth of submergence

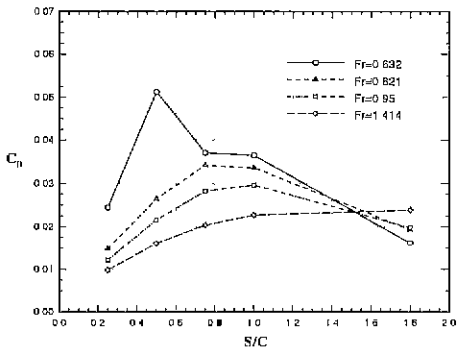

Figure 6: Drag coefficient vs. depth of submergence

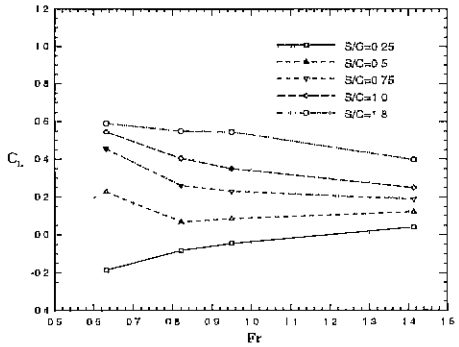

Figure 7: Lift Coefficient vs. Froude number

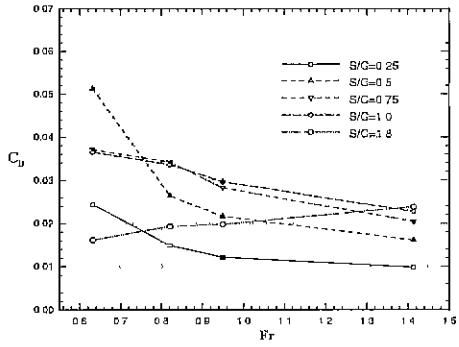

Figure 8: Drag Coefficient vs. Froude number

Figures 7 and 8 present the calculated lift and drag coefficients, respectively, as a function of F_r. For $S/C = 0.75$, 1.0, 1.8 , the lift decreases as the Froude number increases. This may be understood better if we consider the submergence depth normalized by the wave legth corresponding to each Froude number. In other word, the lift decreases as S/λ decreases. For $S/C = 0.25$, the lift is negative for most Froude numbers presented here and decreases as the Froude number decreases. The lift coefficient curve for $S/C = 0.5$ follows a similar trend except the value at $F_r = 0.632$. The drag coefficients appear to decreases as the Froude number increases except those for $S/C = 1.8$ have the opposite behavior. Comparisons of the numerical results with the estimations based on the measured surface pressures are given in Figure 9 and 10 for the lift and drag coefficients for $S/C = 0.25$. An overall good agreement is achieved but there are some discrepancies at $F_r = 0.632$ and 0.604 for the lift and drag coefficients, respectively.

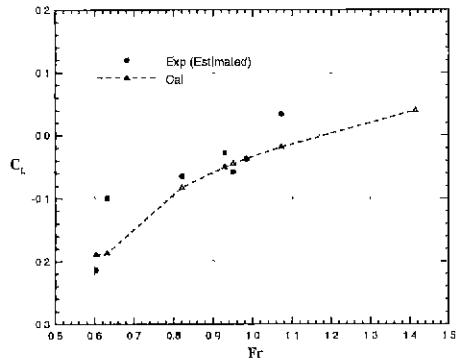

Figure 9: Lift Coefficient vs. Froude number (S/C = 0.25)

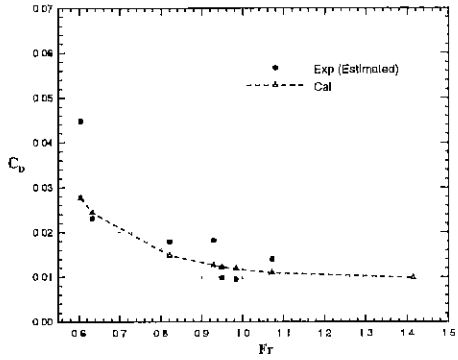

Figure 10: Drag Coefficient vs. Froude number (S/C = 0.25)

3.2 Tandem hydrofoils

The results of tandem hydrofoils are presented for several separation distances between the forward and aft foils to show their interference effect. The forward and aft foils have the same geometry and their angle of attack is 5^o, $F_r = 0.95$ and $S/C = 1.8$. Although no direct comparison can be made due to the lack of experimental information, the computed flows exhibit many interesting features of the interference effects between two hydrofoils in a tandem arrangement.

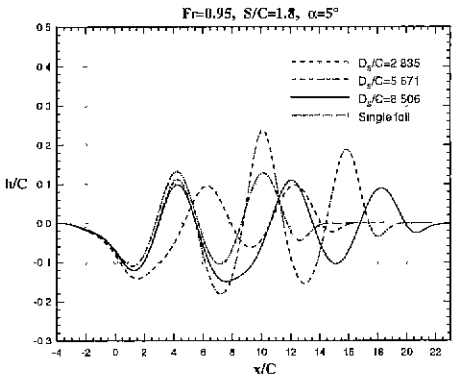

Figure 11: Interference effect for separation distance (wave, D_s/C = 2.835, 5.671, 8.506)

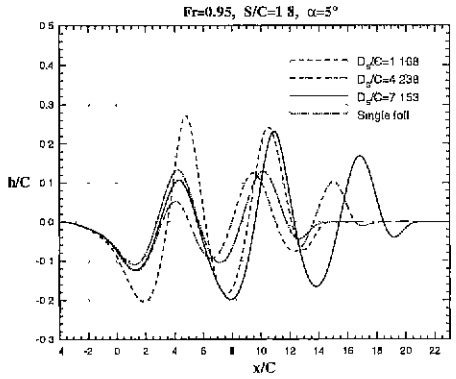

Figure 12: Interference effect for separation distance (wave, D_s/C = 1.168, 4.238, 7.153)

Figure 11 shows the interference effect for the three different separations, i.e., $D_S/C = 2.835$, 5.671, 8.506, where the separation distance D_s is the horizontal distance between the midchord points of the forward and aft hydrofoils. These three separations correspond to $D_S = \lambda/2, \lambda, 1.5\lambda$, respectively. The diminution of the wave is conspicuous for $D_S = 0.5\lambda$. The second and third hollows and humps are salient in the wave profiles for $D_S = \lambda$. For $D_S = 1.5\lambda$, there is a moder-

ate attenuation of the wave. Figure 12 shows the results for $D_S/C = 1.168, 4.238$ corresponding to $D_S = 0.2\lambda, 0.75\lambda, 1.25\lambda$, respectively. The diminution of the wave is evident for $D_S = 0.75\lambda$. For $D_S = 1.25\lambda$, there is a moderate augmentation of the wave. The second and third hollows and humps are considerably enlarged for $D_S = 0.2\lambda$.

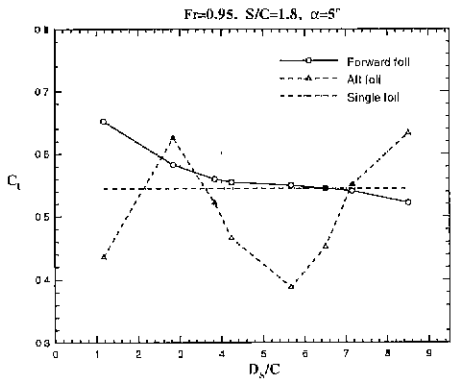

Figure 13: Lift coefficient vs. separation distance

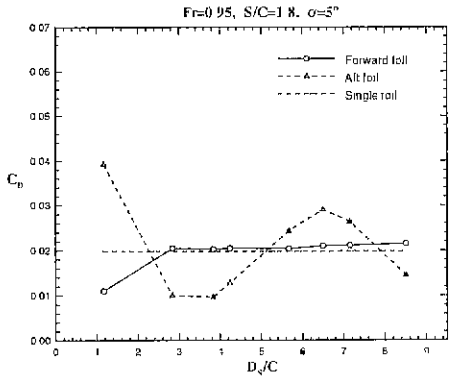

Figure 14: Drag coefficient vs. separation distance

Finally, in Figures 13 and 14, the lift and drag of the forward and aft foils is presented as a function of D_S/C with those of the single foil as the reference. The lift of the forward foil increases monotonously as D_S decreases and it reaches the value with a gain of 18% over that of the single hydrofoil for $D_S/C = 1.168$. The lift coefficient of the aft foil fluctuates with D_S/C . It reaches the peak values with about 14% increase over that of the single hydrofoil for $D_S/C = 2.835$ and 8.506, which corresponds to $D_S = 0.5\lambda$ and 1.5λ, respectively. On the other hand, it reaches the trough values with about 25% decrease from that of the single hydrofoil for $D_S/C = 1.168$ and 5.671 corresponding to, respectively, $D_S = 0.2\lambda$ and λ . The drag coefficient of the aft foil also fluctuates with D_S/C, while the drag of the forward foil is kept almost constant except the sudden decrease for $D_S/C = 1.168$. The former for $D_S/C = 1.168$ becomes 0.04 which is about twice of the drag coefficient of the single hydrofoil. From a point of view for the design of tandem hydrofoils, $D_S/C = 2.835$ or 8.506 may be an optimum separation to maximize the total lift and to minimize the total drag, while $D_S/C = 1.168$ or 4.238 could be a choice for the good stability.

4 Conclusions

In present study, Reynolds-averaged Navier-Stokes equations are numerically solved for the analysis of turbulent flows around a single and tandem hydrofoils advancing under the free surface. Validation of the present method is accomplished by the comparison of the numerical results with the experimental data for a single hydrofoil of a 12% thick Joukowski section. The calculated surface pressures are in good agreement with experiment. A further computational study is carried out to investigate the effect of the submergence depth and the Froude number on the lift and the drag of the hydrofoil. For tandem hydrofoils, computations are performed for several separation distances between the forward and aft foils to investigate the interference effect. The results clearly

show how the lift and drag changes with the separation distance which predominately controls the lifting-body as well as the wave interference effects.

References

BAI, K.J. 1978 A localized finite-element method for two-dimensional steady potential flows with a free surface. J. of Ship Research, **22**, **4**

BAI, K.J. AND HAN, J.H. 1994 A localized finite-element method for nonlinear steady waves due to two-dimensional hydrofoil. J. of Ship Research, **38**, **1**

BALDWIN B.S. AND LOMAX, H. 1978 Thin layer approximation and algebraic model for separated turbulent flows analysis of open water characteristics of a rudder. AIAA Paper, pp. 78-257

DUNCAN, J.H. 1983 The breaking and non-breaking wave resistance of a two-dimensional hydrofoil. J. of Fluid Mechanics, **126**

HINO, T. 1989 Numerical computation of a free surface flow around a submerged hydrofoil by the Euler/Navier-Stokes equations. J. of Society of Naval Architects of Japan, **164**

HINO, T. 1993 A finite-volume method with unstructured grid for free surface flow simulations. Proc. 6th Int'l Conference on Numerical Ship Hydrodynamics

KIM, W.J. 1994 An experimental and computational study on the pressure distribution around a hydrofoil moving under the free surface. Report UCE554-1845D, KRISO, Korea,

KIM, W.J. AND VAN, S.H. 1995 An experimental and computational study on the flow around a hydrofoil with a free surface. J. Hydrospace Technology, **1**, **2**

KOCHIN, N.E. 1951 On the wave-making resistance and lift of bodies submerged in water. Technical and Research Bulletin, SNAME, **1-8**

LEE, S.J. AND KIM, H.T. 1996 Lift of and wave breaking behind a moving submerged body with shallow submergence. J. of Hydrospace Technology, **2**, **2**

PARKIN, B.R., PERRY, B. AND WU, T.Y. 1955 Pressure distribution on a hydrofoil running near the water surface. CIT Hydrodynamics Lab. Report 47-2

SHIN, M.S. AND MORI, K.H. 1989 On the turbulent characteristics and numerical simulation of 2-dimensional sub-breaking waves. J. of Society of Naval Architects of Japan, **165**

SOTIROPOULOS, F. 1991 A primitive variable method for the solution of external and internal incompressible flow-fields. Ph.D. Thesis, Univ. of Cincinnati

VAN, S.H., KIM, W.J. AND KIM, Y.G. 1996 Lift characteristics of 2-dimensional hydrofoil near the free surface. Proc. Korea-Japan Joint Workshop on Ship and Marine Hydrodynamcis,

VISBAL M. AND KNIGHT, D. 1982 Generation of orthogonal and nearly orthogonal coordinates with grid control near boundaries. J. of AIAA, **20**, **3**